communications
earth & environment

ARTICLE

https://doi.org/10.1038/s43247-023-00725-5 OPEN

Reconstructing high-resolution in-situ vertical carbon dioxide profiles in the sparsely monitored Asian monsoon region

Bärbel Vogel [1]✉, C. Michael Volk[2], Johannes Wintel[2,5], Valentin Lauther[2], Rolf Müller [1], Prabir K. Patra [3], Martin Riese [1], Yukio Terao [4] & Fred Stroh[1]

Atmospheric concentrations of the greenhouse gases carbon dioxide and nitrous oxide have increased substantially because of human activities. However, their sources in South Asia, which contribute strongly to the accelerating global growth of carbon dioxide and nitrous oxide, are poorly quantified. Here, we present aircraft measurements with high temporal and vertical resolution up to 20 km during the Asian summer monsoon where rapid upward transport of surface pollutants to greater altitudes occurs. Using Lagrangian model simulations, we successfully reconstruct observed carbon dioxide profiles leading to an improved understanding of the vertical structure of carbon dioxide in the Asian monsoon region. We show that spatio-temporal patterns of carbon dioxide on the Indian subcontinent driven by regional flux variations rapidly propagate to approximately 13 km with slower ascent above. Enhanced carbon dioxide compared to the stratospheric background can be detected up to 20 km. We suggest that the propagation of these signals from the surface to the stratosphere can be used to evaluate transport models and assess carbon dioxide fluxes in South Asia.

[1] Institute of Energy and Climate Research (IEK-7), Forschungszentrum Jülich, Jülich, Germany. [2] Institute for Atmospheric and Environmental Research, University of Wuppertal, Wuppertal, Germany. [3] Research Institute for Global Change, Japan Agency for Marine-Earth Science and Technology (JAMSTEC), Yokohama, Japan. [4] Earth System Division, National Institute for Environmental Studies, Ibaraki, Japan. [5] Present address: Curt-Engelhorn-Centre of Archaeometry gGmbH, Mannheim, Germany. ✉email: b.vogel@fz-juelich.de

The amount of greenhouse gases (GHGs) in the atmosphere such as CO_2 and N_2O has increased worldwide because of anthropogenic emissions. Atmospheric carbon dioxide (CO_2) increased substantially since the beginning of the industrial era (by more than 45% since about 1750). In particular, the rapid increase of anthropogenic CO_2 emissions in South Asia contributes strongly to the acceleration of its growth rate, e.g., the anthropogenic CO_2 emission rate from India was the fourth highest worldwide in 2017 (behind China, the USA and the European Union); For example India's fossil CO_2 emissions increased by $+5.1\%\ yr^{-1}$ for the last decade (2009–2018) compared to a global increase of $+1.3\%\ yr^{-1}$[1].

Global human-induced emissions of N_2O which are dominated by contributions from the agricultural sector i.e., by the use of nitrogen-based fertilisers increased by 30% between 1980 and 2016 in particular in agriculture-oriented economies such as India and China[2].

Due to the sparse availability of regional atmospheric observations over the Indian subcontinent there is currently a lack of sufficient coverage of continuous quality-controlled ground-based monitoring stations of GHGs such as CO_2 and N_2O. Continuous ground-based measurements of CO_2 and N_2O are essential to derive the spatial and temporal variations of CO_2 and N_2O emissions, for providing adequate boundary conditions for model simulations, and to infer long-term trends of their emissions[3–9].

Our study shows the great impact that an expansion of this network with continuous measurements would have. This would allow for realistic 3D simulations of CO_2 in the South Asian atmosphere and provides added value to atmospheric and climate modelling as well as to satellite-based CO_2 monitoring.

Methods to constrain CO_2 surface-atmosphere fluxes comprise a variety of bottom-up and top-down approaches[10]. The latter, also called inverse approaches employ a transport model with a priori fluxes that are adjusted so that simulated concentrations best fit observations[11,12]. Such approaches are frequently hampered by the limited temporal and spatial availability of ground based, airborne or space-borne observations.

In state-of-the-art chemistry transport models, the transport of air parcels differs because different methods (Eulerian, Lagrangian), different vertical velocities (kinematic, diabatic) and different meteorological reanalyses (e.g., ERA5, ERA-Interim, JRA-55) are used to drive the models[13,14]. Further, the implementation of convection and irreversible mixing differs from model to model.

Here we use a unique set of CO_2 and N_2O aircraft measurements at high temporal and vertical resolution up to ~ 20 km altitude (corresponding to ~ 55 hPa or ~ 475 K potential temperature) obtained in the Asian summer monsoon where CO_2 and N_2O airborne measurements were hitherto only available up to ~ 12 km (~ 180 hPa)[15–18].

From about June to September, the Asian summer monsoon constitutes a seasonally persistent zonally restricted circulation pattern transporting climate-relevant emissions rapidly from the surface boundary layer to greater altitudes, i.e., to the lower stratosphere[19–23]. The Asian summer monsoon is associated with deep convection over the Indian subcontinent and an anticyclonic flow in the upper troposphere and lower stratosphere (UTLS) over the Asian monsoon region spanning from northeast Africa to the Pacific[21]. Air parcels are uplifted quickly by convection followed by slow diabatic uplift in the UTLS superimposed by the anticyclonic flow, while in other regions within the tropical transition layer (TTL) the heating rates are in general smaller during boreal summer[23]. Further, the thermal tropopause as well as isentropes (in log-pressure altitude coordinates) are enhanced in the region of the Asian monsoon anticyclone compared to the residual TTL[24]. The higher the air parcels are located above the level of maximum convective outflow (≈ 360 K ≈ 13 km), the larger the contribution of air masses is from outside the Asian monsoon anticyclone (i.e., from the stratospheric background) to the upward spiraling flow[23].

We demonstrate that the combination of ground-based observations on the Indian Subcontinent (in particular at Nainital) and Lagrangian transport modelling provides realistic 3D CO_2 distributions in the Asian Monsoon region up to 20 km altitude. This, in turn, is a prerequisite for a realistic representation of associated radiative effects in atmospheric and climate models and a solid foundation for satellite-based monitoring of CO_2 fluxes based on inverse modelling approaches.

Results

Measurements. In general ground-based measurements of CO_2 on the Indian subcontinent reflect the seasonality of carbon exchange in the northern terrestrial biosphere, which is mostly related to the seasonality of the vegetation activity by photosynthetic CO_2 absorption by plants in this latitude range[5,9]. However measured CO_2 values depend in detail strongly on local natural sources and sinks as well as—even more important—on anthropogenic emissions such as combustion of fossil fuels, land use change and biomass burning[5,7–9,25].

The net CO_2 uptake by plants is the net balance of photosynthesis and respiration; photosynthesis dominates over respiration in summer, but only during daytime and respiration dominates in winter and during nighttime. During the pre-monsoon period (March–May) a seasonal CO_2 maximum and during the monsoon period (June–September) a seasonal minimum is found at different stations on the Indian subcontinent[5,8,9,26] resulting in a negative phase (decreasing concentration of CO_2) during April–August and a positive phase (increasing concentration of CO_2) during September–March.

Figure 1 shows the seasonal variability of ground-based CO_2 and N_2O measurements at different sites during 2016 and 2017 (details see Methods; geographical positions are shown in Fig. 2). Stations in the northern hemisphere such as Nainital (India) and Mt. Waliguan (China) show one clear seasonal maximum in March–May and one seasonal minimum in June–September. CO_2 in Comilla (Bangladesh) has two seasonal minima per year, in February–March and September, corresponding to crop cultivation activities that depend on regional climatic conditions in contrast to Nainital that only has one clear minimum in September[9]. Air masses over the Indian subcontinent were transported from the Indian Ocean region during summer (monsoon season) and from the inland during winter, therefore observations in Nainital are strongly affected by anthropogenic emissions from the Indo-Gangetic Plain during summer. Anthropogenic emissions, e.g., of CO_2, in the Indo-Gangetic Plain are higher compared to other regions in India[9] caused by the dense concentration of industries (e.g., thermal power plants, steel plants, refineries) as well as by the very high population density in this area[27]. Thus air masses transported long-range from the south to Nainital, can uptake these emission while passing over the Indo-Gangetic Plain[9].

The CO_2 maximum at Mauna Loa is measured about 4 weeks later compared to measurements at sites in continental Asia (Fig. 1). The seasonal cycle of CO_2 at Mauna Loa (Hawaii) is representative for marine northern-hemispheric background air. CO_2 observations at Cape Matutala (Samoa) are representative for southern-hemispheric background air and are shifted about half a year compared to the northern hemisphere due to seasons determining vegetation growing periods.

The seasonal variability of N_2O on the northern Indian subcontinent is consistent with the application of nitrogen fertiliser,

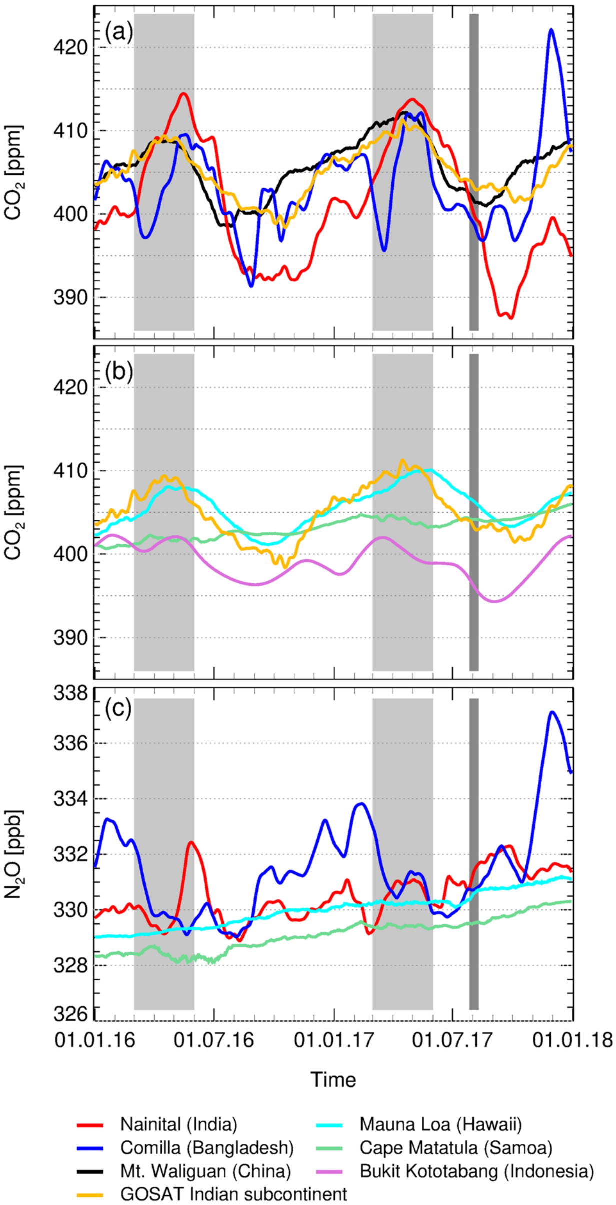

Fig. 1 Temporal variability of ground-based CO_2 and N_2O. The variability of ground-based CO_2 **a**, **b** and N_2O **c** is shown at different sites in Asia and the Pacific for 2016-2107 (details see Methods). Ground-based CO_2 measurements from different continental stations in Asia **a** and from different stations in the Inter-Tropical Convergence Zone **b** are compared (geographical positions see Fig. 2). In addition, the seasonal variability of CO_2 over the northern Indian subcontinent (mean value between 20–30°N and 75–95°E) of the lowest model level at 975 hPa of the GOSAT-L4B product (details see Methods) for comparison to ground-based CO_2 measurements is shown. The pre-monsoon period (March–May) when a seasonal CO_2 maximum is expected is high-lighted (light-grey) as well as the period of the StratoClim aircraft campaign during monsoon 2017 (dark-grey).

biomass burning and change in monsoonal/trade winds[9,28]. Therefore, the N_2O mixing ratios in Nainital and Comilla are in general higher compared to sites in the Pacific (Mauna Loa, Cape Matutala; see Fig. 1c). Higher N_2O values are found in Comilla located in the eastern Indo-Gangetic Plain compared to Nainital located in the western Indo-Gangetic Plain (Fig. 1c).

Column-averaged CO_2 from satellite measurements show also a distinct seasonal cycle of CO_2 over India with a negative phase from northern hemisphere late spring to summer and a positive phase from autumn to spring[26,29]. The seasonal variability of CO_2 over the Indian subcontinent (mean value between 10–35°N and 65–95°E) at the ground (the lowest model level at 975 hPa) as estimated by the GOSAT-L4B product (details see Methods) is compared to ground-based CO_2 measurements in Fig. 1a, b. The GOSAT-L4B product is a model simulation using CO_2 surface fluxes inferred from column-averaged satellite measurements (details see Methods); the lowest model level of GOSAT-L4B is closest to the inferred CO_2 surface fluxes and is not strongly influenced by the tracer transport of the underlying transport model. The GOSAT-L4B mean value has a similar seasonal variability as other CO_2 ground-based measurements on the northern hemisphere (Mt. Waliguan, Nainital, Mauna Loa), however its amplitude is lower than for the ground-based measurements in Nainital demonstrating the limitations of GOSAT-L4B data compared to in situ measurements.

In the frame of the StratoClim project funded by the European Commission, a measurement campaign using the Russian Geophysica high altitude research aircraft was conducted in Kathmandu (Nepal) in summer 2017 (see Fig. 2) to measure a variety of trace gases and aerosol characteristics for the first time in the Asian monsoon anticyclone up to 20 km altitude (corresponding to ~ 55 hPa or ~ 475 K potential temperature)[30]. These StratoClim measurements constitute a unique data set to characterise major processes which dominate particle and trace gas transport from one of the most polluted regions of the world into the lower stratosphere.

High-resolution CO_2 and N_2O profiles measured in-situ (Fig. 3; details see Methods) reflect the seasonal variability of CO_2 and N_2O at ground level (see Fig. 1). Although CO_2 has a strong diurnal cycle near the ground, CO_2 concentrations are relatively independent from diurnal variations in the upper troposphere and lower stratosphere (UTLS). CO_2 is chemically inert in the troposphere and stratosphere and can be used as an age tracer considering time periods of several months[31–33].

N_2O is essentially inert in the troposphere and has no significant sinks at the surface of the Earth. The critical region for N_2O loss is the tropical middle stratosphere (24–40 km)[34] where destruction of N_2O occurs via photolysis and reaction with excited atomic oxygen ($O(^1D)$). The decrease of measured N_2O profiles above 400 K potential temperature (Fig. 3) indicates mixing with older stratospheric air that has descended from higher altitudes[35]. The high-resolution CO_2 and N_2O vertical profiles up to 20 km altitude presented here yield a unique insight into their altitude dependency in the region of the Asian monsoon.

Both the seasonality of CO_2 and its long lifetime make it an appropriate chemical tracer for a reconstruction along backward trajectories over several months because chemical processes can be ignored. Therefore, CO_2 is very well suited to analyse in detail transport pathways, transport times and mixing in the Asian summer monsoon anticyclone and beyond using backward trajectory calculations over a simulation period of about one year.

Transport times and air mass origin. Trajectory calculations were performed based on the Chemical Lagrangian Model of the Stratosphere (CLaMS)[36–38] (details see Methods). CLaMS diabatic backward trajectories driven by high resolution ERA5 reanalysis[39] were started along the entire flight paths (every 1 sec) of all Geophysica flights to infer the transport time from the location of the measurement back to the time when the air parcel was released at the model boundary layer (BL; details see Methods). The trajectories are calculated back to 1 June 2016 and are analysed within different time periods to identify the source regions at the model BL depending on season (see Table 1).

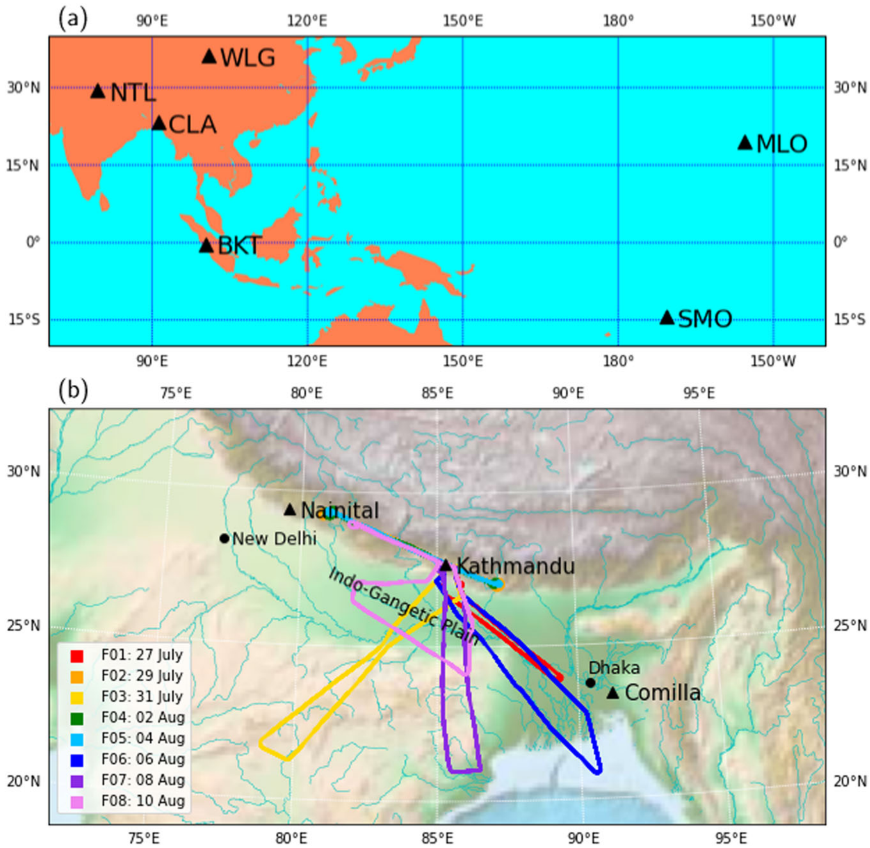

Fig. 2 Regional map of the measurement sites for greenhouse gases and of the aircraft measurements on the Indian subcontinent. The locations of the measurement sites for greenhouse gases in Nainital (NTL, India) Comilla (CLA, Bangladesh), Mt. Waliguan (WLG, China), Bukit Kototabang (BKT, Indonesia), Mauna Loa (MLO, Hawaii) and Samoa (SMO, Cape Matatula) **a** and the flight paths of the eight local scientific flights (F01-F08) by the high altitude research aircraft Geophysica **b** are shown. The scientific flights were carried out every second day from Kathmandu (Nepal) between 27 July and 10 August 2017.

However, most air parcels encounter the model BL within a few months of backward transport (e.g., 64% of all trajectories reach the model BL during the monsoon season 2017).

As expected, simulated transport times increase with the altitude of sampled air parcels (Fig. 3). However, there is also a strong variability of transport times between individual air parcels at the same level of potential temperature indicating mixing of air masses of different transport times or of different ages.

For the CO_2 reconstruction it is essential to determine the location where the back trajectories intersect the model BL so that they can be tagged with the closest ground-based measurement. Figure 4 shows the frequency distribution for different seasons of the locations where the air parcels were released at the model BL. Most air parcels were released at the model BL during monsoon 2017 (64%), pre-monsoon 2017 (14%), and winter 16/17 (6%). Minor fractions are from post-monsoon 2016 (3%) and monsoon 2016 (3%). In summary, 90% of the air parcels were released at the model BL after 1 June 2016, the other 10% is aged air.

During monsoon 2017 most air parcels were released in the northern part of the Indian subcontinent, the Tibetan Plateau, Bay of Bengal and eastern China (Fig. 4a). A cluster of air parcels at the model BL is also found in the western Pacific caused by typhoon activity (details see ref. [30]). During pre-monsoon 2017 the origins are shifted towards the tropics to the northern Inter-Tropical Convergence Zone (ITCZ) e.g., over the Indian Ocean and the western Pacific. For winter 16/17, the origins move further to the south to the southern Inter-Tropical Convergence Zone (ITCZ) mostly over the Warm Pool region, northern Australia and western Pacific. The contributions from post-monsoon 2016 and monsoon 2016 are minor. In summary, we show that the patterns of the frequency distribution depend strongly on the considered season and hence from the age of air.

Based on the frequency distribution shown in Fig. 4 and on the limited availability of CO_2 ground-based measurements in the region of the Asian monsoon and in the tropics from 2016 to 2017 a regional mask was developed where different BL regions (Fig. 5) are defined. This regional mask allows the CO_2 at the model BL to be prescribed depending on the BL region.

To estimate which back-trajectory length is best for CO_2 reconstruction the fractions of air released at the model BL are inferred depending on different time intervals adjusted to the seasons on the Indian subcontinent (see Table 1). For our approach to reconstruct CO_2 profiles from ground-based measurements it is important to use backward trajectories with a high fraction of air from the model BL. Figure 6 shows the fraction of air from the model BL, splitted into the BL regions shown in Fig. 5. Further, fractions of the free atmosphere are indicated (Fig. 6). The fractions of air are accumulated back to starting times of different seasons: monsoon 2017 (a), pre-monsoon 2017 (b), winter 16/17 (c), post-monsoon 2016 (d), monsoon 2016 (e). The longer the trajectories the higher are the contributions from the model BL and the lower are the fractions from the free atmosphere.

Considering all air parcels released at the model BL after the beginning of winter 16/17 yields a fraction greater than 90% up to levels of potential temperature of 400 K (Fig. 6c). Thus air masses from three seasons, monsoon 2017, pre-monsoon 2017 and winter 16/17, have to be taken into account. Above 400 K mixing

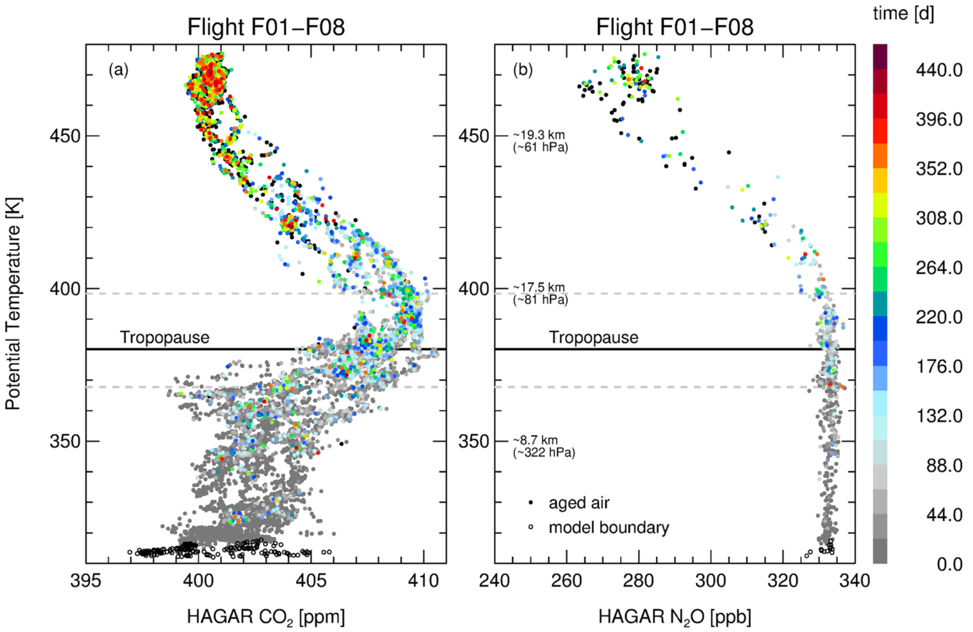

Fig. 3 Airborne CO_2 and N_2O measurements from the StratoClim campaign in Kathmandu (Nepal) during July and August 2017. Each air parcel is coloured by the transport time from the model boundary layer (BL) to the time of measurements inferred by Lagrangian back-trajectory calculations. Air parcels located in the model BL as well as aged air (air located in the free atmosphere on 1 June 2016) are marked. The number of air parcels is determined by the different temporal resolution of the CO_2 **a** and N_2O **b** measurements (details see Methods). In addition, the mean WMO tropopause[71] as well as the lowest and highest tropopause (grey dashed lines) over Kathmandu during the flight days are shown.

Table 1 Time periods and age of air of considered seasons on Indian subcontinent.

Season	Time period	Start time	Age of air
Monsoon 2017	June–September 2017	1 June 2017	~ 2 months
Pre-monsoon 2017	March–May 2017	1 March 2017	~ 2–5 months
Winter 16/17	December 2016 - February 2017	1 Dec 2016	~ 5–8 months
Post-monsoon 2016	October–November 2016	1 Oct 2016	~ 8–10 months
Monsoon 2016	June–September 2016	1 June 2016	~ 10–14 months
Aged air	older than 1 June 2016		> 14 months

The analysis of CLaMS back-trajectories (see Methods) is performed back until the start time of each season. For each season air parcels that were released at the model boundary layer (BL) are analysed. The longest simulation time is back until 1 June 2016 (~1 year). Air parcels that are located in the free atmosphere on 1 June 2016 are considered as aged air.

with older air masses successively occurred and the fraction from the model BL rapidly decreases. Between 440 K and 480 K 50% of the air is younger than 1 June 2016; the other half is aged air.

At core altitudes of the Asian monsoon between ~ 360 K and 410 K the main contributions are from BL regions of the Indian Subcontinent, Bangladesh, the Tibetan Plateau and adjacent regions on the continental and maritime northern hemisphere. At the top of the Asian monsoon anticyclone (above 420 K) the contribution from the free atmosphere (stratospheric background) is dominating. The longer the trajectories the more contributions from model BL regions from the tropical southern hemisphere, the Warm Pool region, and the maritime northern hemisphere play a role. After a simulation period of ~ 14 months (until 1 June 2016) the contributions from the tropical southern hemisphere and the maritime northern hemisphere are roughly equal in the lower stratosphere.

Sensitivity of CO_2 reconstruction on observation sites. Reconstructed vertical CO_2 profiles using CLaMS Lagrangian trajectory calculations are determined by CO_2 prescribed at the model BL and by the transport of air parcels along the trajectories driven by ERA5 reanalysis and diabatic vertical velocities. To infer the impact of different ground-based measurements, of mixing of air from inside the Asian monsoon anticyclone with air from the (stratospheric) background as well as of the trajectory lengths different sensitivity studies (cases) are performed for CO_2 reconstruction.

To analyse how the seasonal variability of different CO_2 ground-based measurements is reflected in CO_2 reconstruction, CO_2 is reconstructed prescribing CO_2 for all air parcels released at the model BL using one specific ground-based site ignoring the origin of air parcels at the model BL. All air parcels that were released after 1 June 2016 at the model BL are used and all air parcels from the free atmosphere (mainly stratospheric background) are not considered in this first case (case S1; see Supplementary Discussion (Fig. S1) for the impact of the trajectory length).

In Fig. 7, CO_2 mixing ratios reconstructed in this way are shown as median of 1 K intervals for several measurement sites. The averaging of reconstructed CO_2 in 1 K intervals reflects mixing of air masses originating in different locations in the model BL or having different transport times.

The CO_2 maximum in the UTLS is best reconstructed using Nainital measurements as expected because the majority of the air parcels originate at the BL region of the Indian subcontinent.

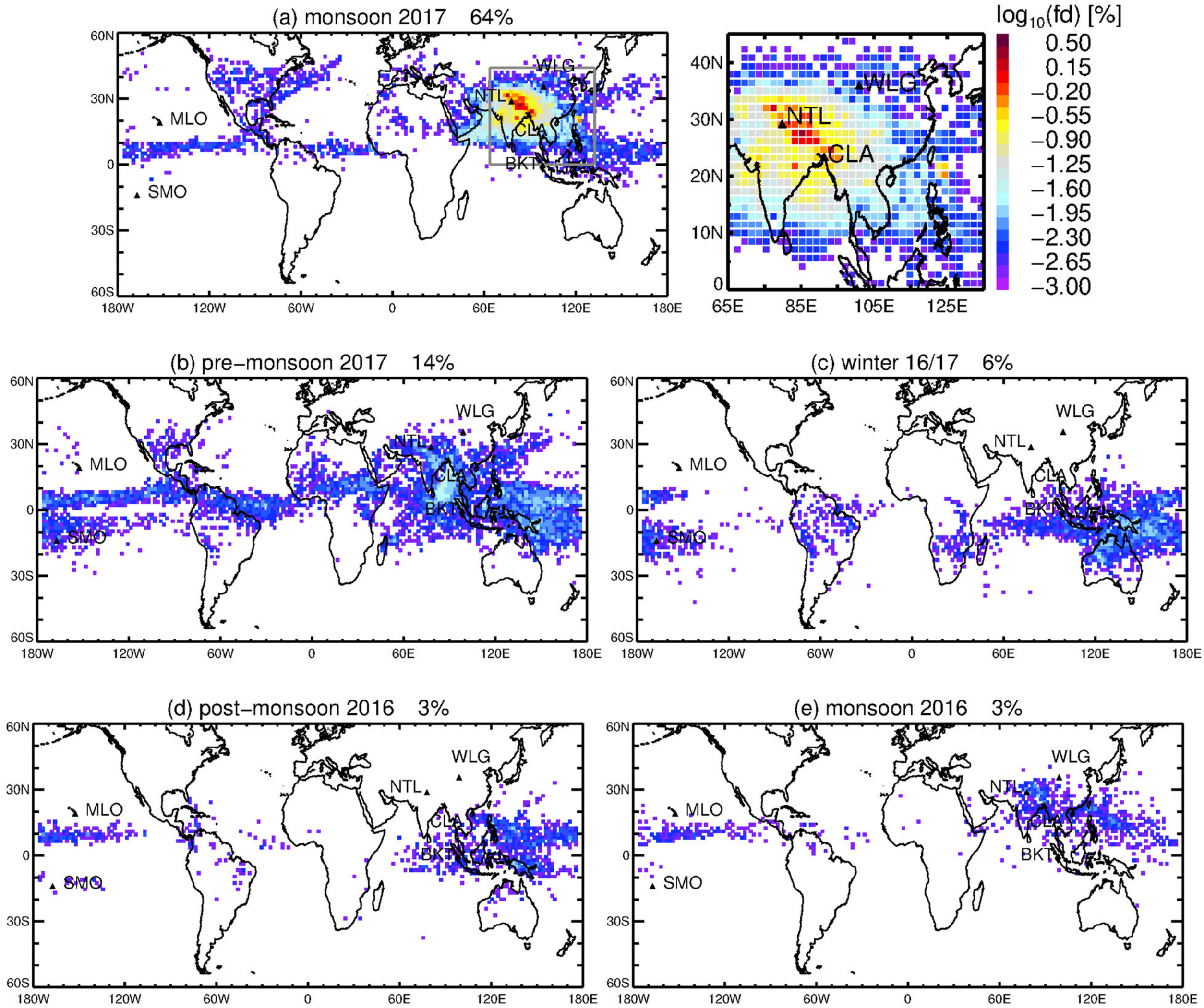

Fig. 4 Frequency distribution (fd) of the air mass origins at the model boundary layer (BL). Frequency distribution (number of trajectories normalised by the total number of trajectories started along the flight path) of the locations where the air parcels were released at the model BL (see Methods). Trajectories driven by ERA5 reanalysis were started along the entire flight paths (every 1 sec) of all eight Geophysica flights. The frequency distributions are shown for different seasons (representing different ages of air; see Table 1): monsoon 2017 **a** (a zoom of Asia marked as grey box is shown right beside), pre-monsoon 2017 **b**, winter 16/17 **c**, post-monsoon 2016 **d** and monsoon 2016 **e**. The frequency distribution is calculated in longitude-latitude bins of 2.0° × 1.5°. The percentages indicate the fraction of air parcels released at the model BL within a certain season. In summary, 90% of the air parcels were released at the model BL after 1 June 2016, the other 10% originates from aged air. The patterns of the frequency distribution depend strongly on the considered season. Further, the locations of different ground-based measurement sites in Asia and the Pacific are shown (details see Table 2).

In Fig. 6c, it is shown that up to 410 K mainly air parcels released at the model BL after 1 December 2016 contribute to measured CO_2 profiles. Above 410 K, air masses from the (stratospheric) background and from the northern and southern Intertropical Convergence Zone (ITCZ) contribute strongly to the composition of air probed during StratoClim within the Asian monsoon anticyclone in July and August 2017 at its top and beyond (see Fig. 4). Contributions from India are minor above ~ 410 K (Fig. 6), therefore reconstructed CO_2 at this altitude has to be prescribed by measurements from other regions (e.g., Mouna Loa, Samoa and Bukit Kototabang). A mixture of air from different origins and with different ages needs to be considered for a full CO_2 reconstruction which will be discussed in the next Section.

N_2O can be reconstructed in a similar way as CO_2 using the ground-based measurements from Nainital, Comilla, Mauna Loa and Samoa. Because of the in 2016/17 low seasonal variability of N_2O at the ground (Fig. 1c) compared to variability of vertical N_2O profiles below 400 K (Fig. 3b), the reconstruction below 400 K results in a constant vertical profile (Fig. 7b). Because chemical loss of N_2O in the stratosphere cannot be represented in the approach of back-trajectory reconstruction, the reconstructed and measured N_2O profiles start to diverge between 400 K and 410 K indicating mixing with aged stratospheric air above this altitude.

CO_2 reconstruction. For a reliable reconstruction of measured vertical CO_2 profiles over the entire altitude range, both accurate back-trajectory calculations are required as well as precise CO_2 concentrations at the ground. For the latter purpose, a regional mask was developed (case S2) where CO_2 is prescribed in the model BL depending on different BL regions (Fig. 5).

Figure 8a shows reconstructed CO_2 using a regional mask for back-trajectory calculations until 1 December 2016 neglecting the contributions from the free atmosphere (case S2a). The comparison with measured in situ CO_2 profiles shows a

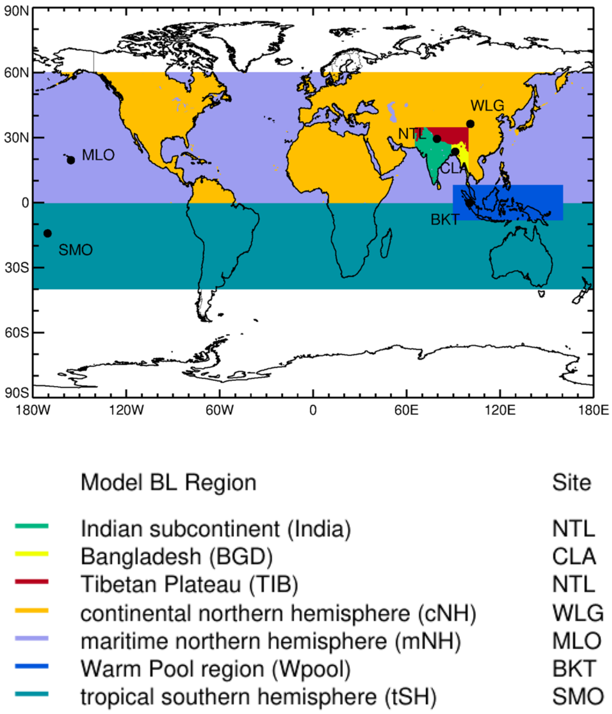

Fig. 5 Regional mask to reconstruction CO_2. Regional mask to reconstruction CO_2 using CO_2 ground-based measurements at different sites in Asia and the Pacific. In each model boundary layer (BL) region (marked by different colours) CO_2 is prescribed from one specific measurement site: tropical southern hemisphere (tSH) by Samoa (SMO), Indian subcontinent (India) by Nainital (NTL), Bangladesh (BGD) by Comilla (CLA), Tibetan Plateau (TIB) by Nainital (NTL), maritime northern hemisphere (mNH) by Mauna Loa (MLO), continental northern hemisphere (cNH) by Mt. Waliguan (WLG) and Warm Pool region (Wpool) by Bukit Kototabang (BKT).

very good agreement from the model BL up to ~ 410 K. Above ~ 410 K, the fraction of trajectories from the free atmosphere (mainly stratospheric background) has to be taken into account (Fig. 6c). Figure 8b shows reconstructed CO_2 as in case S2a but using in addition GOSAT-L4B CO_2 data for the fraction of air parcels from the free atmosphere (case S2b). Here, for each 1 K interval the median of all air parcels considering both the fraction from the model BL as well as from the free atmosphere is calculated. This approach allows the mixing of air at the top of the Asian monsoon anticyclone between air mass from the boundary layer and air from (stratospheric) background to be considered. Air from the boundary layer above 400 K originates mainly in the southern and northern ITCZ. Extreme low CO_2 values from ground-based measurements in the Warm Pool region have to be taken into account to reconstruct CO_2 in this altitude range.

Thus at this altitude range, there is mixing of air from the model BL with air from the stratospheric background. Reconstructed CO_2 from the model BL is higher than the measured CO_2 profile and air from the stratospheric background has lower CO_2 values (not shown here) than the measured CO_2 profile. Thus only the mixing of these two different air masses allows measured CO_2 profiles to be reconstructed accurately. Using this approach our findings yield a good overall agreement between measured and reconstructed CO_2 profiles, however differences are found at potential temperature levels between 430 K and 470 K, but still within the range of the 25 and 75 percentile.

The sensitivity of the quality of the reconstruction of CO_2 (case S2b) on the employed trajectory length was tested. They can be too short (and thus miss contributions from the model BL) or too long (resulting in higher uncertainties). The longer the back-trajectory calculations the higher the altitudes of the end points of the trajectories from the free atmosphere. Based on the latter trajectories CO_2 is reconstructed from GOSAT-L4B data that are providing CO_2 values up to 10 hPa. The longer the trajectories the

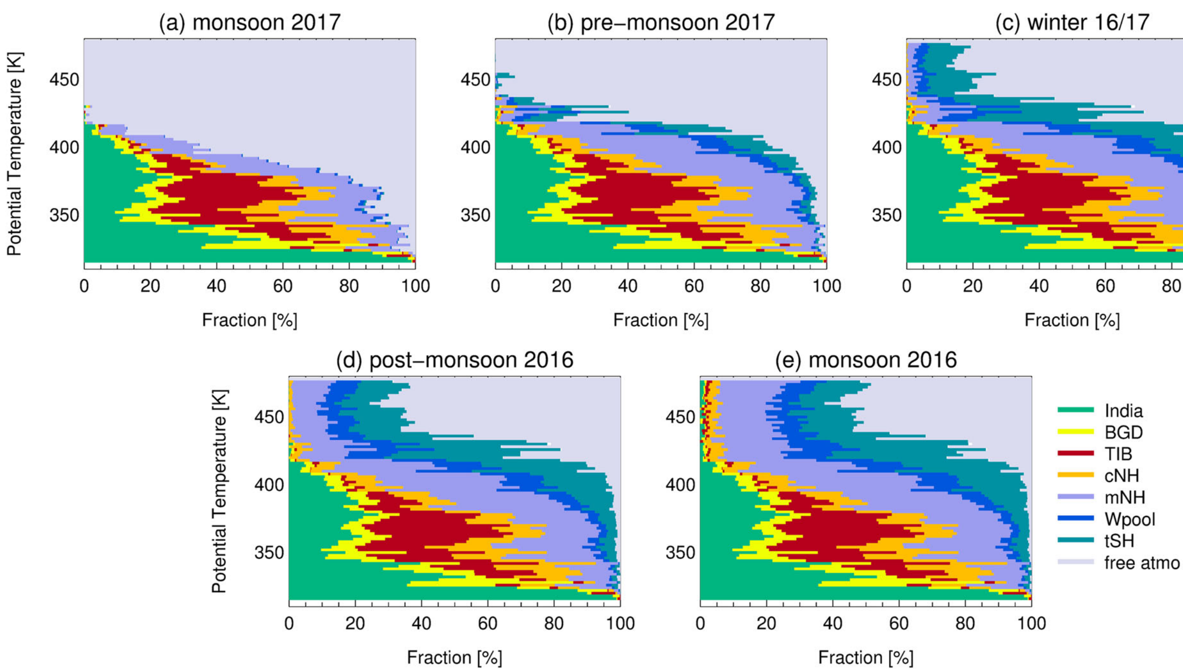

Fig. 6 The fraction of air from the model boundary layer (BL) and the free atmosphere. The fraction from the model BL and from the free atmosphere is calculated from all backward trajectories started along the Geophysica flight tracks averaged in 2 K intervals and accumulated back to the start times of different seasons: monsoon 2017 **a**, pre-monsoon 2017 **b**, winter 16/17 **c**, post-monsoon 2016 **d**, monsoon 2016 **e** (detailed start times are listed in Table 1). In **e**, the fraction of air referred to as the free atmosphere corresponds to the fraction of `aged air' defined in Table 1. The fraction of air from the model BL is divided in the different BL regions as shown in Fig. 5.

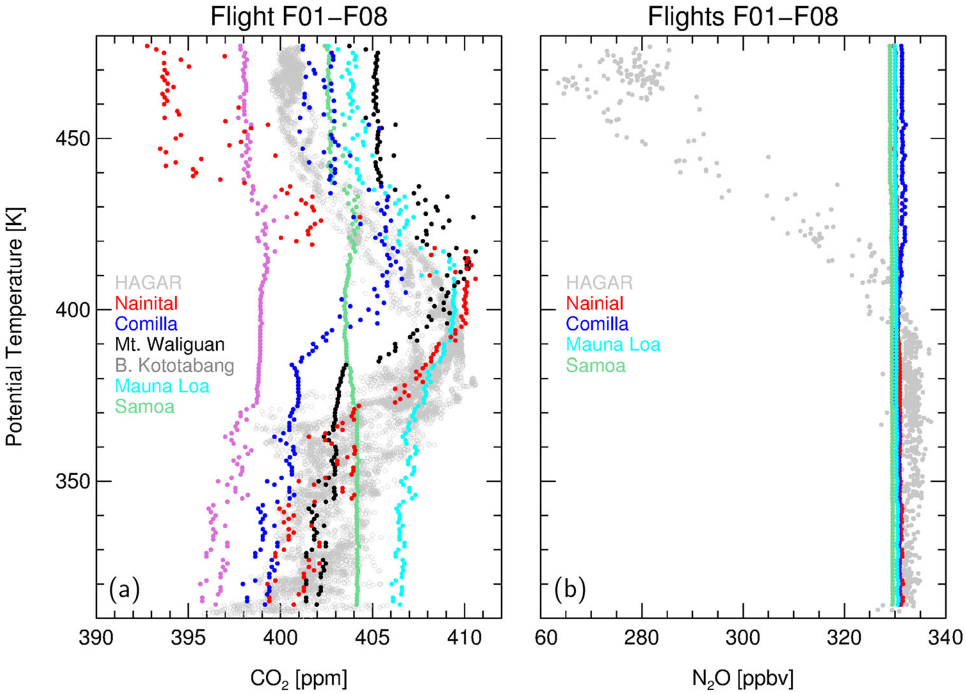

Fig. 7 CO_2 and N_2O airborne measurements and reconstructed CO_2 and N_2O (case S1). Vertical profiles of CO_2 **a** and N_2O **b** airborne measurements (research flights F01-F08; HAGAR; light grey) are reconstructed using ground-based measurements from different sites in Asia and the Pacific indicated by different colours (locations of the different sites are shown in Fig. 2). CO_2 mixing ratios from ground-based measurements are prescribed at the time when each trajectory reach the model BL and subsequently passively transported along each trajectory to the location of the measurement (details see Methods). The reconstructed CO_2 values are shown as median in 1 K intervals (based on trajectories started every one second along the flight path). The seasonal variability of CO_2 ground-based measurements is visible in the vertical profile of reconstructed CO_2. Trajectories that do not reach the model BL until the beginning of the monsoon season 2016 on 1 June 2016 (i.e., air from the free atmosphere; mainly from the stratospheric background) are not considered here.

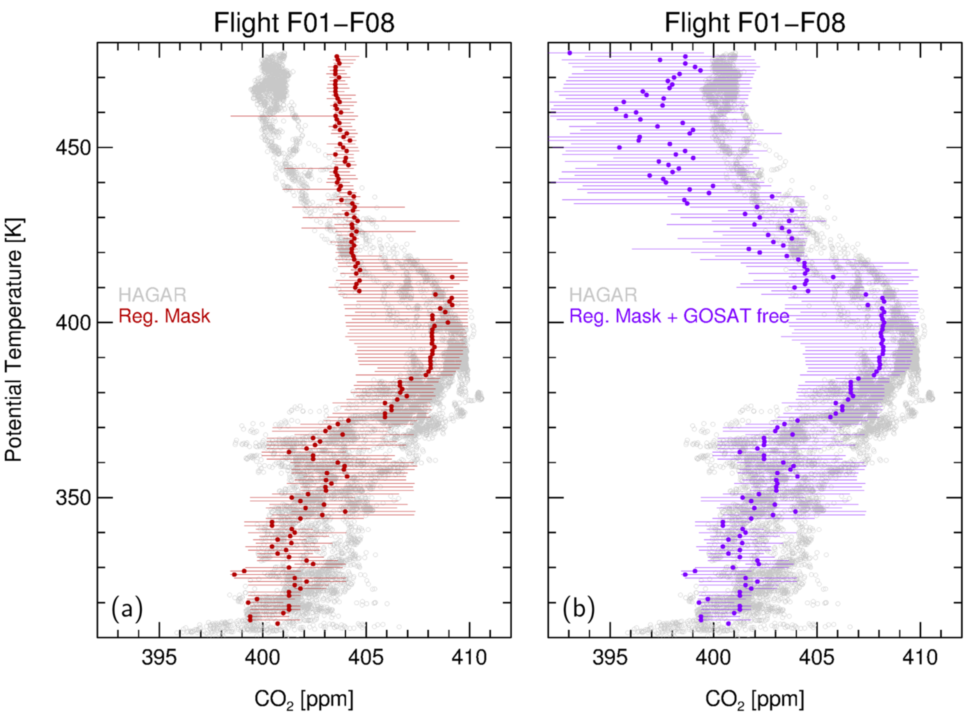

Fig. 8 Reconstructed CO_2 using back-trajectory calculations until 1 December 2016 compared to HAGAR CO_2 airborne measurements. Reconstructed CO_2 is shown as median calculated from all trajectories until 1 December 2016 in 1 K intervals for research Flights F01-F08. **a** Reconstructed using regional mask shown in Fig. 5 for the fraction of trajectories ending in the model BL (case S2a). **b** Reconstructed CO_2 as in case S2a but using in addition GOSAT-L4B CO_2 data for the fraction of trajectories ending in the free atmosphere, mainly from stratospheric background (case S2b). Bars indicate the range between the 25 and 75 percentile.

Table 2 Observational sites of CO_2 and N_2O in South Asia and in the western Pacific.

Site	Label	Measurement method	Location	Elevation [m.a.s.l.]	Remarks
Nainital (India)	NTL	flask samples (weekly)	29.4°N 79.5°E	1940	influenced by the Indo-Gangetic Plain in summer
Comilla (Bangladesh)	CLA	flask samples (weekly)	23.4°N 91.2°E	30	dominated by agricultural activities
Mt. Waliguan (China)	WLG	surface in situ (daily)	36.3°N 100.9°E	3810	Asian background
Mauna Loa (Hawaii)	MLO	surface in situ (daily)	19.5°N 155.6°W	3397	maritime background air northern Hemisphere
Samoa (Cape Matatula)	SMO	surface in situ (daily)	14.2°S 170.6°W	77	background air southern Hemisphere
Bukit Kototabang (Indonesia)	BKT	flask samples (monthly)	0.2°S 100.3°E	864	equatorial rain forest, fully humid

For each site, measurement method, geographical location, elevation and some remarks are given.

more the altitudes of the end points exceeds the altitude of the pressure level of 10 hPa and the CO_2 values are here extrapolated to higher pressure levels which increases the uncertainties of reconstructed CO_2 (see Supplementary Discussion (Fig. S1) for a detailed discussion on this issue). We decided to show back-trajectories to 1 December 2016, because for this date up to 410 K reconstructed CO_2 is determined solely by CO_2 prescribed at the model BL and by the transport of air parcels along the back-trajectories. Here, the uncertainties regarding the CO_2 extrapolation to higher pressure levels are negligible.

However, above 410 K the quality of the GOSAT-L4B needs also to be taken into account for an assessment of the quality of CO_2 reconstruction. GOSAT-L4B data depend on CO_2 fluxes at the Earth's surface (GOSAT-L4A data), on model resolution as well as on vertical transport in the used atmospheric transport model (NIES-TM; details see Methods). In Fig. 1a, b, it is shown that GOSAT-L4B data of the lowest model level at 975 hPa over the Indian subcontinent during the seasonal maximum in March-May 2017 are somewhat lower than the ground-based measurements in Nainital. Therefore, reconstructing CO_2 from GOSAT-L4B (lowest level) CO_2 by CLaMS trajectories yield lower CO_2 values compared to case S2 in the UTLS caused by the lower CO_2 seasonal maximum at the ground; see Supplementary Discussion (Fig. S2) for a detailed discussion on this issue as well as a direct comparison of GOSAT-L4B CO_2 data with HAGAR CO_2.

The contribution of CH_4 oxidation in the stratosphere is estimated to be much lower (0.09% at 470 K) than the variability of reconstructed CO_2 in this altitude region, therefore, CO_2 from CH_4 oxidation is not considered in our approach.

Discussion/conclusions

Unique airborne measurements of the GHGs CO_2 and N_2O at altitudes of the Asian monsoon anticyclone are presented. High-resolution in situ CO_2 profiles are observed up to 20 km altitude and are reconstructed by back-trajectory calculations. Below 410 K, reconstructed CO_2 using CLaMS Lagrangian trajectory calculations is determined solely by CO_2 prescribed at the model BL based on measurements and by the transport of air parcels along the trajectories using high-resolution ERA5 reanalysis and diabatic vertical velocities. Above 410 K, the agreement with in situ CO_2 profiles is improved by taking into account the stratospheric background. Our findings show that the Lagrangian transport in CLaMS using diabatic vertical velocities and driven by the European Centre for Medium-Range Weather Forecasts' new high-resolution reanalysis ERA5 is very well suited for CO_2 reconstruction (see Supplementary Discussion Fig. S2 for further details on this issue) and could be applied to other CO_2 aircraft observations.

The good agreement of reconstructed CO_2 with in situ CO_2 profiles speaks for the benefits of uninterrupted surface measurements in Nainital and Comilla. It implies that a greater number of continuous ground-based measurements of CO_2 and also other GHGs in South Asia, in particular on the Indian subcontinent, would be a great asset for atmospheric and climate modelling and for improving estimates of regional-scale surface-atmosphere CO_2 fluxes, which are needed to develop policies mitigating the continued growth of fossil fuel emissions[40].

State-of-the art global inversion systems assimilating mostly ground-based in situ observations currently do not well constrain the annual net CO_2 flux of South Asia, their estimates ranging from -0.5 to $+0.4$ Pg C/year[41], which reflects the lack of CO_2 observations in that region. For example, the current release of the Carbon-Tracker (CT2019B)[42], though based on 460 time series datasets from around the world, does not include ground-based measurements from the Indian subcontinent after 2013 (when CO_2 monitoring in Cape Rama ended). Thus not surprisingly, the CO_2 distribution at the ground over South Asia during summer 2017 is not well represented in CarbonTracker (see Supplementary Discussion Fig. S3 for further discussion on this issue). As a consequence, when using CarbonTracker CO_2 as the lower boundary condition, the vertical distribution of CO_2 over South Asia during summer 2017 could not be well represented in 3-dimensional model simulations[43] in contrast to our approach (see Supplementary Discussion Figs. S4 and S5 for reconstruction of each StratoClim research flight F01-F08).

Recent advances in space-based remote sensing have greatly increased spatial and temporal coverage of column-averaged CO_2 and driven the development of inverse systems employing these satellite data, alone or in conjunction with in situ data[44–47]. In fact, GOSAT-L4B data is a simulation product based on CO_2 fluxes derived from a joint inversion of column-averaged GOSAT and ground-based CO_2 data. However, the GOSAT and OCO-2 satellites do not provide measurements in persistently cloudy regions, including South Asia during the monsoon season[44,46]. The need for improvements in this region is obvious from the comparison of GOSAT-L4B with CO_2 ground-based measurements in Nainital and Comilla as well as with CO_2 vertical profiles measured by the HAGAR instrument during the StratoClim campaign (Fig. S2). The misrepresentation of the observed 3D structure in the GOSAT-L4B and Carbon-Tracker simulation reflects the large void of data in the South Asia region and/or limitations in model transport, and thus casts doubt on the reliability of the derived regional CO_2 fluxes.

Our study shows that during the Asian Monsoon spatio-temporal patterns of CO_2 on the Indian Subcontinent driven by regional flux variations rapidly propagate to approximately 13 km with slower ascent above. Enhanced CO_2 compared to the stratospheric background can be detected up to 20 km. However in the stratosphere, the fraction of air originating on the Indian subcontinent is low compared to contributions from the tropics and of aged air from the stratosphere. We suggest that the propagation of these signals from the surface to the stratosphere constitutes a stringent test for atmospheric transport simulations and thus the data presented here provide an unprecedented opportunity for CO_2 inversion systems to critically evaluate model transport and assess the derived CO_2 fluxes in South Asia. High-resolution CO_2 profiles can further be used to study stratosphere-troposphere-exchange processes as well as the intra-seasonal variability during the Asian monsoon season.

South Asia is the most densely populated part of the world and here further increasing anthropogenic emissions are expected in the future due to the strong growth of Asian economies. We conclude, the quantification of CO_2 and other GHG surface fluxes and their temporal changes would highly benefit from an expansion of the ground-based GHG measuring network in South Asia complemented by regular vertical CO_2 soundings, which could be achieved at comparatively low cost by AirCore sampling and subsequent laboratory analysis (a method requiring only moderate instrumentation collecting air in a very long lightweight stainless-steel tube, usable on a variety of platforms including small balloons)[48]. This would also provide a solid base for policy action.

Methods

Ground-based measurements. Ground-based measurements of atmospheric mole fractions of CO_2 and N_2O at different observation sites in South Asia, in particular, on the Indian subcontinent, and from the western Pacific (locations of all sites are shown in Fig. 2) are used to reconstruct observed CO_2 vertical profiles during the StratoClim campaign. Measurements of CO_2 and N_2O at Nainital (India) and Comilla (Bangladesh)[9,49–52] were provided through the Global Environmental Database, Center for Global Environmental Research, National Institute for Environmental Research (NIES). Measurements at Mt. Waliguan (China)[53], Bukit Kototabang (Indonesia)[54], Mauna Loa (Hawaii)[55], https://gml.noaa.gov/aftp/data/trace_gases/ and Samoa (Cape Matatula)[55], https://gml.noaa.gov/aftp/data/trace_gases/ are provided by the World Data Centre for Greenhouse Gases (WDCGG) (https://gaw.kishou.go.jp). Further details about each site such as location, elevation and measurement method are summarised in Table 2.

CO_2 and N_2O data at different sites are provided on different time scales (daily, weekly or monthly). For CO_2 and N_2O reconstruction it is required to interpolate all ground-based measurements on a daily time grid over the time period from 2016 to 2017. To get a comparable variability of the interpolated data, they are smoothed with a boxcar average of a width of 30 days as shown in Fig. 1.

Airborne measurements. HAGAR[56,57] is a multi-tracer in situ instrument operated by the University of Wuppertal. Apart from CO_2 and N_2O, it also provides simultaneous in situ measurements of CH_4, CFC-12, CFC-11, H-1211, SF_6, and H_2. Except for CO_2, which is measured at high time resolution (3 to 5 s) by non-dispersive infrared absorption (NDIR), all the other species were measured by gas chromatography with electron capture detection (GC/ECD) every 90 s. The instrument is calibrated every 7.5 min during flight with either of two standard gases, which are inter-calibrated in the laboratory with standards provided by NOAA GML. For StratoClim the accuracy of the measurements was estimated to be about 2 ppb for N_2O and about 0.2 ppm for CO_2.

HAGAR data were referenced to standards provided by NOAA and are based on the CO_2 WMO X2007 scale and the N_2O NOAA-2006 scale. The data can be converted to the current CO_2 WMO X2019 and N_2O NOAA-2006a scales using the following equations, which are based on reassigned standard values on the current scales:

$$X2019 = 1.00033 * X2007 + 0.0467 \quad (1)$$

$$2006a = 0.99841 * X2006 + 0.587 \quad (2)$$

These conversions amount to small positive shifts of about 0.18 ppm for CO_2 and 0.05 to 0.17 ppm for N_2O.

GOSAT-L4B data product. CO_2 mixing ratios are used from the Greenhouse gases observing satellite (GOSAT) (http://www.gosat.nies.go.jp/en/about_5_products.html) launched 2009 by the Japan Aerospace Exploration Agency (JAXA)[58] L4B data product to reconstruct measured CO_2 profiles.

GOSAT observes infrared light using the Thermal And Near-infrared Sensor for carbon Observation (TANSO) instrument which consists of a Fourier Transform Spectrometer (FTS) and a Cloud and Aerosol Imager (CAI). The FTS measures the solar radiation reflected from the ground by sensors at three short-wave infrared bands (0.76, 1.6 and 2.0 µm) as well as the ground and atmospheric radiation at a wide thermal infrared band (5.5–14.3 µm). FTS has a instantaneous field of view determined by the nadir footprint size of 10.5 km in diameter. Absorption spectra are obtained from TANSO where interferences of clouds and aerosols are small and column abundances of CO_2 over observation points can be calculated. Thus vertically integrated concentrations of CO_2 were used to estimate sources and sinks of CO_2, i.e., surface fluxes (GOSAT-L4A data product), by performing inverse simulations. Monthly fluxes of CO_2 in GOSAT-L4A data are estimated for 42 terrestrial and 22 oceanic regions (64 regions total)[44].

We use the GOSAT-L4B data product (V02.07) of atmospheric CO_2 concentrations which has 17 vertical levels up to 10 hPa (in atmosphere hybrid sigma pressure coordinates), a horizontal resolution of 2.5° × 2. 5° and a time step of six hours driven by GOSAT-L4A surface fluxes[58].

The GOSAT-L4B data product is a result of a global atmospheric tracer transport simulation using NIES atmospheric tracer transport model (NIES-TM v08.1i) using a 32-level hybrid isentropic grid[59]. Vertical velocities are calculated in isentropic coordinates above 350 K using a climatology of adiabatic heating/cooling rates derived from monthly mean values on pressure levels of the JRA-25 reanalysis[60] provided by the Japan Meteorological Agency (JMA).

CLaMS trajectory calculations. Trajectory calculations were performed using the the Chemical Lagrangian Model of the Stratosphere (CLaMS)[36–38] which was developed with the aim to study transport and chemical processes throughout the troposphere and stratosphere in the presence of strong tracer gradients. Here, CLaMS diabatic backward trajectories were started along the entire flight paths (every 1 sec) of all Geophysica flights conducted over the northeastern part of the Indian subcontinent. Overall ~ 110,000 back-trajectories are calculated between 9000 and 16000 per flight depending on the flight lengths.

In the CLaMS model, potential temperature is used as the vertical coordinate when the pressure is less than about 300 hPa, (i.e., in the upper troposphere and in the stratosphere); when the pressure is greater than about 300 hPa (more accurately, for pressure p exceeding a reference level of $p/p_{surface} = 0.3$), a pressure-based orography-following hybrid coordinate (in units of K) is used[38]. Above about 300 hPa, the vertical velocity is determined solely by the total heating rate[38,61]. Total diabatic heating rates include clear-sky radiative heating, cloud radiation, latent heat release, as well as turbulent and diffusive heat transport for the upper troposphere and stratosphere are used from ERA5 reanalysis[61]. ERA5 reanalysis[39] is a high-resolution atmospheric data set with 137 vertical levels up to 0.01 hPa, a horizontal resolution of ~ 31 km (T_L 639) and a hourly time resolution. We retrieved the data at 0.3° × 0. 3° horizontal grid. Caused by the much higher spatio-temporal resolution of ERA5 reanalysis[39] compared to earlier reanalyses, a much better representation of convective updraft and tropical cyclones is realised[62–64]. Trajectories are considered ending in the model boundary layer, when they are located for the first time below about 2–3 km above surface considering orography (i.e., the vertical hybrid pressure–potential–temperature coordinate $\zeta \leq 120$ K) in the paper referred to as 'model boundary layer (BL)'details see e.g., [22,23]. CLaMS trajectory calculations are very well suited to analyse the transport in the region of the Asian monsoon and were utilised using both ECMWF' prior reanalysis ERA-Interim[23,65–70] as well as the new ERA5 data set[30,63].

CO_2 reconstruction approach. CO_2 mixing ratios from ground-based observations measured during the time when the CLaMS back-trajectories reach the model BL are used. For that the ground-based observations are interpolated on a daily grid. This calculated CO_2 defines the reconstructed CO_2 at the start point of the trajectory along the Geophysica flight path.

A regional mask was developed (setup S2) where CO_2 is prescribed in the model BL depending on different geographical regions (see Fig. 5). In each of these geographical regions (in the paper referred to as 'BL region') CO_2 is prescribed using one specific measurement site, e.g., trajectories ending in the BL region marked in green and dark-red (roughly Indian Subcontinent and Tibetan Plateau) are prescribed using ground-based measurements from Nainital and the BL region marked in yellow (roughly Bangladesh) is prescribed using ground-based measurements from Comilla. Unfortunately the coverage of ground-based measurements of CO_2 over the Indian subcontinent in 2016 to 2017 is sparse, therefore only data from Nainital and Comilla are available.

Data availability

The StratoClim data can be downloaded from the HALO database at https://halo-db.pa.op.dlr.de/mission/101. For more details on HAGAR CO_2 and N_2O measurements please contact C. Michael Volk (M.Volk@uni-wuppertal.de). Ground-based CO_2 and N_2O from Nainital and Comilla were provided through National Institute for Environmental Research (NIES) available under[49–52]. Ground-based CO_2 and N_2O measurements from other sites can be downloaded from the World Data Centre for Greenhouse Gases (WDCGG) (https://gaw.kishou.go.jp) and GOSAT-L4B CO_2 data under (https://data2.gosat.nies.go.jp/index_en.html). The ERA5 tropopause is available under Hoffmann, Lars; Spang, Reinhold, 2021, "Reanalysis Tropopause Data Repository", https://datapub.fz-juelich.de/slcs/tropopauseVersion 1.2.

Code availability

The CLaMS trajectory code is available on the GitLab server https://jugit.fz-juelich.de/clams/CLaMS.

Received: 10 June 2022; Accepted: 21 February 2023;
Published online: 24 March 2023

References

1. Friedlingstein, P. et al. Global carbon budget 2019. *Earth System Science Data* **11**, 1783–1838 (2019).
2. Tian, H. et al. A comprehensive quantification of global nitrous oxide sources and sinks. *Nature* **586**, 248–256 (2020).
3. Bhattacharya, S. et al. Trace gases and CO_2 isotope records from Cabo de Rama, India. *Curr. Sci.* **97**, 1336–1344 (2009).
4. Tiwari, Y. K., Vellore, R. K., Ravi Kumar, K., van der Schoot, M. & Cho, C.-H. Influence of monsoons on atmospheric CO_2 spatial variability and ground-based monitoring over India. *Sci. Total Environ.* **490**, 570–578 (2014).
5. Lin, X. et al. Long-lived atmospheric trace gases measurements in flask samples from three stations in India. *Atmos. Chem. Phys.* **15**, 9819–9849 (2015).
6. Chandra, N., Lal, S., Venkataramani, S., Patra, P. K. & Sheel, V. Temporal variations of atmospheric CO_2 and CO at Ahmedabad in western India. *Atmos. Chem. Phys.* **16**, 6153–6173 (2016).
7. Sreenivas, G. et al. Influence of meteorology and interrelationship with greenhouse gases (CO_2 and CH_4) at a suburban site of India. *Atmos. Chem. Phys.* **16**, 3953–3967 (2016).
8. Mahata, K. S. et al. Seasonal and diurnal variations in methane and carbon dioxide in the Kathmandu Valley in the foothills of the central Himalayas. *Atmos. Chem. Phys.* **17**, 12573–12596 (2017).
9. Nomura, S. et al. Measurement report: regional characteristics of seasonal and long-term variations in greenhouse gases at Nainital, India, and Comilla, Bangladesh. *Atmos. Chem. Phys.* **21**, 16427–16452 (2021).
10. Crisp, D. et al. How well do we understand the land-ocean-atmosphere carbon cycle? *Rev. Geophys.* **60**, e2021RG000736 (2022).
11. Peylin, P. et al. Daily CO_2 flux estimates over Europe from continuous atmospheric measurements: 1, inverse methodology. *Atmos. Chem. Phys.* **5**, 3173–3186 (2005).
12. Thompson, R. L. et al. Top-down assessment of the Asian carbon budget since the mid 1990s. *Nat. Commun*. **7**, (10724) https://doi.org/10.1038/ncomms10724 (2016).
13. Bergman, J. W., Fierli, F., Jensen, E. J., Honomichl, S. & Pan, L. L. Boundary layer sources for the Asian anticyclone: regional contributions to a vertical conduit. *J. Geophys. Res.* **118**, 2560–2575 (2013).
14. Ploeger, F. et al. How robust are stratospheric age of air trends from different reanalyses? *Atmos. Chem. Phys.* **19**, 6085–6105 (2019).
15. Schuck, T. J. et al. Greenhouse gas relationships in the Indian summer monsoon plume measured by the CARIBIC passenger aircraft. *Atmos. Chem. Phys.* **10**, 3965–3984 (2010).
16. Patra, P. K. et al. Carbon balance of South Asia constrained by passenger aircraft CO_2 measurements. *Atmos. Chem. Phys.* **11**, 4163–4175 (2011).
17. Sawa, Y., Machida, T. & Matsueda, H. Aircraft observation of the seasonal variation in the transport of CO_2 in the upper atmosphere. *J. Geophys. Res.*117 (D5) https://doi.org/10.1029/2011JD016933 (2012).
18. Umezawa, T. et al. Seasonal evaluation of tropospheric CO_2 over the Asia-Pacific region observed by the CONTRAIL commercial airliner measurements. *Atmos. Chem. Phys.* **18**, 14851–14866 (2018).
19. Mason, R. B. & Anderson, C. E. The development and decay of the 100-mb. summertime anticyclone over southern Asia. *Monthly Weather Rev.* **91**, 3–12 (1963).
20. Randel, W. J. & Park, M. Deep convective influence on the Asian summer monsoon anticyclone and associated tracer variability observed with Atmospheric Infrared Sounder (AIRS). *J. Geophys. Res.* **111**, https://doi.org/10.1029/2005JD006490 (2006).
21. Park, M., Randel, W. J., Gettleman, A., Massie, S. T. & Jiang, J. H. Transport above the Asian summer monsoon anticyclone inferred from Aura Microwave Limb Sounder tracers. *J. Geophys. Res.* **112**, https://doi.org/10.1029/2006JD008294 (2007).
22. Vogel, B., Günther, G., Müller, R., Grooß, J.-U. & Riese, M. Impact of different Asian source regions on the composition of the Asian monsoon anticyclone and of the extratropical lowermost stratosphere. *Atmos. Chem. Phys.* **15**, 13699–13716 (2015).
23. Vogel, B. et al. Lagrangian simulations of the transport of young air masses to the top of the Asian monsoon anticyclone and into the tropical pipe. *Atmos. Chem. Phys.* **19**, 6007–6034 (2019).
24. Vogel, B. et al. Long-range transport pathways of tropospheric source gases originating in Asia into the northern lower stratosphere during the Asian monsoon season 2012. *Atmos. Chem. Phys.* **16**, 15301–15325 (2016).
25. Tiwari, Y. K. et al. Carbon dioxide observations at Cape Rama, India for the period 1993–2002: implications for constraining Indian emissions. *Current Science* **101**, 1562–1568 (2011).
26. Krishnapriya, M. et al. Seasonal variability of tropospheric CO_2 over India based on model simulation, satellite retrieval and in-situ observation. *J. Earth. Syst. Sci.*129 (211) https://doi.org/10.1007/s12040-020-01478-x (2020).
27. Fadnavis, S., Ravi Kumar, K., Tiwari, Y. K. & Pozzoli, L. Atmospheric CO_2 source and sink patterns over the Indian region. *Annales Geophysicae* **34**, 279–291 (2016).
28. Patra, P. K. et al. Forward and Inverse Modelling of Atmospheric Nitrous Oxide Using MIROC4-Atmospheric Chemistry-Transport Model. *J. Meteorol. Soc. Japan Ser. II* **100**, 361–386 (2022).
29. Kunchala, R. K. et al. Spatio-temporal variability of XCO2 over Indian region inferred from Orbiting Carbon Observatory (OCO-2) satellite and Chemistry Transport Model. *Atmosph. Res.* **269**, 106044 (2022).
30. Stroh, F. & StratoClim-Team. First detailed airborne and balloon measurements of microphysical, dynamical, and chemical processes in the Asian Summer Monsoon Anticyclone: Overview and Selected Results of the 2016/2017 StratoClim field campaigns. *Atmos. Chem. Phys*. (2023).
31. Boering, K. A. et al. Stratospheric mean ages and transport rates from observations of carbon dioxide and nitrous oxide. *Science* **274**, 1340–1343 (1996).
32. Andrews, A. E. et al. Mean age of stratospheric air derived from in situ observations of CO_2, CH_4 and N_2O. *J. Geophys. Res.* **106**, 32295–32314 (2001).
33. Ray, E. A. et al. Age spectra and other transport diagnostics in the North American monsoon UTLS from SEAC^{4}RS in situ trace gas measurements. *Atmos. Chem. Phys.* **22**, 6539–6558 (2022).
34. Prather, M. J. et al. Measuring and modeling the lifetime of nitrous oxide including its variability. *J. Geophys. Res.* **120**, 5693–5705 (2015).
35. Volk, C. M. et al. Quantifying transport between the tropical and mid-latitude lower stratosphere. *Science* **272**, 1763–1768 (1996).
36. McKenna, D. S. et al. A new Chemical Lagrangian Model of the Stratosphere (CLaMS): 1. Formulation of advection and mixing. *J. Geophys. Res.* **107**, 4309 (2002).
37. McKenna, D. S. et al. A new Chemical Lagrangian Model of the Stratosphere (CLaMS): 2. Formulation of chemistry scheme and initialization. *J. Geophys. Res.* **107**, 4256 (2002).
38. Pommrich, R. et al. Tropical troposphere to stratosphere transport of carbon monoxide and long-lived trace species in the Chemical Lagrangian Model of the Stratosphere (CLaMS). *Geosci. Model Dev.* **7**, 2895–2916 (2014).
39. Hersbach, H. et al. The ERA5 global reanalysis. *Q. J. R. Meteorol. Soc.* **146**, 1999–2049 (2020).
40. Peters, G. P. et al. Carbon dioxide emissions continue to grow amidst slowly emerging climate policies. *Nat. Clim. Chang.* **10**, 3–6 (2020).
41. Kondo, M. et al. State of the science in reconciling top-down and bottom-up approaches for terrestrial CO_2 budget. *Global Change Biology* **26**, 1068–1084 (2020).
42. Jacobson, A. R. et al. CarbonTracker Documentation CT2019B release. Tech. Rep., NOAA - Global Monitoring Laboratory https://gml.noaa.gov/ccgg/carbontracker/CT2019B_doc.php#tth_sEc7.1 (2020).
43. Konopka, P. et al. Tropospheric transport and unresolved convection: numerical experiments with CLaMS 2.0/MESSy. *Geosci. Model Dev.* **15**, 7471–7487 (2022).
44. Maksyutov, S. et al. Regional CO_2 flux estimates for 2009–2010 based on GOSAT and ground-based CO_2 observations. *Atmos. Chem. Phys.* **13**, 9351–9373 (2013).
45. Houweling, S. et al. An intercomparison of inverse models for estimating sources and sinks of co_2 using gosat measurements. *J. Geophys. Res.* **120**, 5253–5266 (2015).
46. Philip, S. et al. OCO-2 satellite-imposed constraints on terrestrial biospheric CO_2 fluxes over South Asia. *J. Geophys. Res.* **127**, e2021JD035035 (2022).
47. Peiro, H. et al. Four years of global carbon cycle observed from the Orbiting Carbon Observatory 2 (OCO-2) version 9 and in situ data and comparison to OCO-2 version 7. *Atmos. Chem. Phys.* **22**, 1097–1130 (2022).
48. Karion, A., Sweeney, C., Tans, P. & Newberger, T. AirCore: an innovative atmospheric sampling system. *J. Atmosph. Oceanic Technol.* **27**, 1839–1853 (2010).
49. Terao, Y. et al. Atmospheric xarbon dioxide dry air mole fraction at Comilla, Bangladesh. NIES (2022). Ver.2022.0 (Last updated: 2022/03/01). https://www.nies.go.jp/doi/10.17595/20220301.002-e.html.
50. Terao, Y. et al. Atmospheric nitrous oxide dry air mole fraction at Comilla, Bangladesh. NIES (2022). Ver.2022.0 (Last updated: 2022/03/01). https://www.nies.go.jp/doi/10.17595/20220301.010-e.html.
51. Terao, Y. et al. Atmospheric carbon dioxide dry air mole fraction at nainital, india. NIES (2022). Ver.2022.0 (Last updated: 2022/03/01). https://www.nies.go.jp/doi/10.17595/20220301.001-e.html.
52. Terao, Y. et al. Atmospheric nitrous oxide dry air mole fraction at nainital, india. NIES (2022). Ver.2022.0 (Last updated: 2022/03/01). https://www.nies.go.jp/doi/10.17595/20220301.009-e.html.
53. Fang, S. X. et al. In situ measurement of atmospheric CO_2 at the four WMO/GAW stations in China. *Atmos. Chem. Phys.* **14**, 2541–2554 (2014).

54. Dlugokencky, E., Mund, J., Crotwell, A., Crotwell, M. & Thoning, K. Atmospheric Carbon Dioxide Dry Air Mole Fractions from the NOAA GML Carbon Cycle Cooperative Global Air Sampling Network 1968-2020, Version: 2021-07-30. Tech. Rep., National Oceanic and Atmospheric Administration (NOAA), Global Monitoring Laboratory (GML), Boulder, Colorado, USA (2021).
55. Thoning, K. W., Crotwell, A. M. & Mund, J. W. Atmospheric Carbon Dioxide Dry Air Mole Fractions from continuous measurements at Mauna Loa, Hawaii, Barrow, Alaska, American Samoa and South Pole. 1973-2021, Version 2022-05 National Oceanic and Atmospheric Administration (NOAA), Global Monitoring Laboratory (GML), Boulder, Colorado, USA. https://doi.org/10.15138/yaf1-bk21 (2022).
56. Volk, C. et al. In situ tracer measurements in the tropical tropopause region during APE-THESEO, In *Eur. Comm. Air Pollut. Res. Report*. Vol. **73**, 661–664 (2000).
57. Homan, C. D. et al. Tracer measurements in the tropical tropopause layer during the AMMA/SCOUT-O3 aircraft campaign. *Atmos. Chem. Phys.* **10**, 3615–3627 (2010).
58. Matsunaga, T. & Maksyutov, S. (eds.). *A Guidebook on the Use of Satellite Greenhouse Gases Observation Data to Evaluate and Improve Greenhouse Gas Emission Inventories, Satellite Observation Center*. National Institute for Environmental Studies, Japan (2018).
59. Belikov, D. A. et al. Simulations of column-averaged CO_2 and CH_4 using the NIES TM with a hybrid sigma-isentropic (σ-Θ) vertical coordinate. *Atmos. Chem. Phys.* **13**, 1713–1732 (2013).
60. Onogi, K. et al. The JRA-25 reanalysis. *J. Met. Soc. Jap.* **85**, 369–432 (2007).
61. Ploeger, F. et al. The stratospheric Brewer–Dobson circulation inferred from age of air in the ERA5 reanalysis. *Atmos. Chem. Phys.* **21**, 8393–8412 (2021).
62. Hoffmann, L. et al. From ERA-Interim to ERA5: the considerable impact of ECMWF's next-generation reanalysis on Lagrangian transport simulations. *Atmos. Chem. Phys.* **19**, 3097–3124 (2019).
63. Li, D. et al. Dehydration and low ozone in the tropopause layer over the Asian monsoon caused by tropical cyclones: Lagrangian transport calculations using ERA-Interim and ERA5 reanalysis data. *Atmos. Chem. Phys.* **20**, 4133–4152 (2020).
64. Legras, B. & Bucci, S. Confinement of air in the Asian monsoon anticyclone and pathways of convective air to the stratosphere during the summer season. *Atmos. Chem. Phys.* **20**, 11045–11064 (2020).
65. Vogel, B. et al. Fast transport from southeast Asia boundary layer sources to northern Europe: rapid uplift in typhoons and eastward eddy shedding of the Asian monsoon anticyclone. *Atmos. Chem. Phys.* **14**, 12745–12762 (2014).
66. Li, D. et al. Impact of typhoons on the composition of the upper troposphere within the Asian summer monsoon anticyclone: the SWOP campaign in Lhasa 2013. *Atmos. Chem. Phys.* **17**, 4657–4672 (2017).
67. Li, D. et al. High tropospheric ozone in Lhasa within the Asian summer monsoon anticyclone in 2013: influence of convective transport and stratospheric intrusions. *Atmos. Chem. Phys.* **18**, 17979–17994 (2018).
68. Hanumanthu, S. et al. Strong day-to-day variability of the Asian Tropopause Aerosol Layer (ATAL) in August 2016 at the Himalayan foothills. *Atmos. Chem. Phys.* **20**, 14273–14302 (2020).
69. Li, D. et al. Tropical cyclones reduce ozone in the tropopause region over the Western Pacific: an analysis of 18 years ozonesonde profiles. *Earth's Future* **9**, 1–9 (2021).
70. Lauther, V. et al. In situ observations of CH_2Cl_2 and $CHCl_3$ show efficient transport pathways for very short-lived species into the lower stratosphere via the Asian and the North American summer monsoon. *Atmos. Chem. Phys.* **22**, 2049–2077 (2022).
71. Hoffmann, L. & Spang, R. An assessment of tropopause characteristics of the ERA5 and ERA-Interim meteorological reanalyses. *Atmos. Chem. Phys.* **22**, 4019–4046 (2022).

Acknowledgements
We are indebted to many local institutions, authorities, as well as individuals for making the StratoClim aircraft field campaign a success. We are especially grateful to the Nepalese, Indian, and Bangladeshi authorities for granting clearances as well as the Kathmandu airport authorities for their local support. Strong support by several local science partners is highly appreciated. We thank the Geophysica aircraft crews and pilots without whom these measurements could not have been conducted. The European Commission has granted and funded the StratoClim project within Framework Programme 7 under ENV.2013.6.1-2, Grant agreement No. 603557. The HAGAR operations and data analysis was supported by Thorben Beckert from University Wuppertal and were partly funded by the German Helmholtz Association within the Helmholtz-CAS Joint Research Group No. 307. The Nainital and Comilla measurements were performed by Manish Naja from Aryabhatta Research Institute of Observational Sciences, Md. Kawser Ahmed from University of Dhaka, and Shohei Nomura, Toshinobu Machida, Motoki Sasakawa Hitoshi Mukai from NIES, and supported by the Environment Research and Technology Development Fund (grant nos. JPMEERF20152002, 20182002 and 21S20800) of the Environmental Restoration and Conservation Agency of Japan. Further, we gratefully acknowledge the World Data Centre for Greenhouse Gases (WDCGG) for providing CO_2 and N_2O ground-based measurements in particular Yong Zhang from China Meteorological Administration, Beijing, China; Kirk Thoning, Pieter Tans, Ed Dlugokencky, Xin Lan, Bradley D. Hall, Geoffrey S. Dutton and Stephen A. Montzka from Earth System Research Laboratory (NOAA), Boulder, US. Further, we would like to thank the Japan Aerospace Exploration Agency (JAXA), the National Institute for Environmental Studies (NIES), and the Ministry of the Environment (MOE) for providing the GOSAT L4B-data product in particular Shamil Maksyutov, the NOAA Earth System Research Laboratory for providing CarbonTracker in particular Andy Jacobson, the European Centre for Medium-Range Weather Forecasts (ECMWF) for providing ERA5 reanalyses and the Jülich Supercomputing Centre (JSC; Research Centre Jülich, Germany) for computing time on the supercomputer JUWELS (project CLaMS-ESM). Finally, we acknowledge our colleagues from IEK-7 (Research Centre Jülich) Felix Plöger, Gebhard Günther, Jens-Uwe Grooß, Nicole Thomas, Nicole Spelten and Paul Konopka for support and discussion. The authors thank all reviewers of this paper for their helpful constructive comments.

Author contributions
The StratoClim aircraft campaign was led and coordinated by F.S. C.M.V., J.W., and V.L. were responsible for the measurements and analysis of airborne CO_2 and N_2O profiles. Y.T. provided the ground-based measurements from Nainital and Comilla. The trajectory calculations and CO_2 reconstruction were performed by B.V. P.P. and M.R. provided their expertise. The study was conceived by B.V., C.M.V., and R.M. and the results were discussed by all co-authors. The paper was written by BV with contributions from all co-authors.

Funding
Open Access funding enabled and organized by Projekt DEAL.

Competing interests
The authors declare no competing interests.

Additional information
Supplementary information The online version contains supplementary material available at https://doi.org/10.1038/s43247-023-00725-5.

Correspondence and requests for materials should be addressed to Bärbel Vogel.

Peer review information *Communications Earth & Environment* thanks Nawo Eguchi, Arlyn Andrews and the other, anonymous, reviewer(s) for their contribution to the peer review of this work. Primary Handling Editors: Tuija Jokinen and Clare Davis. Peer reviewer reports are available.